

1 Why models perform differently on particulate matter over East 2 Asia? – A multi-model intercomparison study for MICS-Asia III

3 Jiani Tan¹, Joshua S. Fu¹, Gregory R. Carmichael², Syuichi Itahashi³, Zhining Tao⁴, Kan
4 Huang^{1,5}, Xinyi Dong¹, Kazuyo Yamaji⁶, Tatsuya Nagashima⁷, Xuemei Wang⁸, Yiming Liu⁸,
5 Hyo-Jung Lee⁹, Chuan-Yao Lin¹⁰, Baozhu Ge¹¹, Mizuo Kajino¹², Jia Zhu¹¹, Meigen Zhang¹¹,
6 Hong Liao¹³ and Zifa Wang¹¹

7 ¹ Department of Civil and Environmental Engineering, University of Tennessee, Knoxville, TN, 37996, USA

8 ² Center for Global and Regional Environmental Research, University of Iowa, Iowa City, IA, 52242, USA

9 ³ Central Research Institute of Electric Power Industry, Abiko, Chiba, 270-1194, Japan

10 ⁴ Universities Space Research Association, Columbia, MD, 21046, USA

11 ⁵ Department of Environmental Science and Engineering, Fudan University, Shanghai, 200433, China

12 ⁶ Graduate School of Maritime Sciences, Kobe University, Kobe, Hyogo, 658-0022, Japan

13 ⁷ National Institute for Environmental Studies, Tsukuba, Ibaraki, 305-8506, Japan

14 ⁸ Institute for Environment and Climate Research, Jinan University, Guangzhou, 511443, China

15 ⁹ Department of Atmospheric Sciences, Pusan National University, Busan, 609-735, South Korea

16 ¹⁰ Research Center for Environmental Changes Academia Sinica, 11529, Taiwan

17 ¹¹ Institute of Atmospheric Physics, Chinese Academy of Science, 100029, China

18 ¹² Meteorological Research Institute, Japan Meteorological Agency, 305-0052, Japan

19 ¹³ School of Environmental, Science and Engineering, Nanjing University of Information Science & Technology,
20 Nanjing, 210044, China

21

22 *Correspondence to: Joshua S. Fu (jsfu@utk.edu)*

23 **Abstract.** This study compares the performances of twelve regional chemical transport models
24 (CTM) from the third phase of Model Inter-Comparison Study for Asia (MICS-Asia III) on
25 simulating the particulate matter (PM) over East Asia (EA) in 2010. The participating models
26 include WRF-CMAQ (v4.7.1 and v5.0.2), WRF-Chem (v3.6.1 and v3.7.1), GEOS-Chem, NHM-
27 Chem, NAQPMS and NU-WRF. This study investigates three model processes as the possible
28 reasons for different model performances on PM: (1) Models perform very differently in the gas-
29 particle conversion of sulphur (S) and oxidized nitrogen (N). The model differences in sulphur
30 oxidation ratio (50%) is of the same magnitude as that in SO₄²⁻ concentrations. The gas-particle
31 conversion is one the main reasons for different model performances on fine mode PM. (2) Models
32 without dust emissions/modules can perform well on PM₁₀ at non-dust-affected sites, but largely
33 underestimate (upmost 50%) the PM₁₀ concentrations at dust sites. The implementation of dust
34 emissions/modules in models has largely improved the model accuracies at dust sites (reduce
35 model bias to -20%). However, both the magnitudes and distributions of dust pollutions are not
36 fully captured. (3) The amounts of modelled depositions vary among models by 75%, 39%, 21%

37 and 38% for S wet, S dry, N wet and N dry depositions, respectively. Large inter-model differences
38 are found in the washout ratios of wet deposition (at most 170% in India) and dry deposition
39 velocities (general 0.3-2 cm s⁻¹ differences over inland regions). This study investigates the reasons
40 for different model performances on PM over EA and offers suggestions for future model
41 development.

42 **1 Introduction**

43 Atmospheric pollution due to particulate matter (PM) has raised world-wide attention for its
44 relationship with environmental and public health issues (Fuzzi et al., 2015;Nel, 2005). Fine
45 particles (PM_{2.5}) are associated with cardiovascular and respiratory related cancer and premature
46 deaths (Hoek and Raaschou-Nielsen, 2014;Knol et al., 2009). Outdoor PM_{2.5} pollution is estimated
47 to cause 2.1-5.2 million premature deaths worldwide annually (Lelieveld et al., 2015;Rao et al.,
48 2012;Silva et al., 2013). It accounts for eight percent of global mortality in 2015 and ranks fifth in
49 the global mortality risk (Cohen et al., 2017). East Asia (EA) has been suffering from severe PM
50 pollutions due to anthropogenic emissions and natural dust emissions (Akimoto, 2003). China and
51 India are the top two countries suffering from outdoor air pollution, which altogether account for
52 20% of global mortalities caused by PM_{2.5} exposure in 2010 (Lelieveld et al., 2015). The mixing
53 of dust with anthropogenic pollutants can even enlarge the effects of pollution (Li et al., 2012).
54 However, the impact evaluation of PM pollution is of high uncertainty due to unclearness in the
55 toxicity of PM components (Lippmann, 2014) and difficulty in the measurement and prediction of
56 PM concentrations.

57 For a better understanding of PM pollution, modelling approach has been adopted to study
58 the spatial distributions of PM with the aid of measurements. Multi-model ensemble approach,
59 which interprets modelling results with combined information from several models, has been
60 proven to increase the reliability of model accuracy (Tebaldi and Knutti, 2007). This method has
61 been widely used for studies in Europe (Bessagnet et al., 2016;Vivanco et al., 2017) and at global
62 scales (Lamarque et al., 2013;Galmarini et al., 2017) on air quality issues. The Model Inter-
63 Comparison Study Asia Phase (MICS-Asia) aims at understanding the air quality issues over EA.
64 The first phase of MICS-Asia (MICS-Asia I) was carried out in the 1990s with eight regional
65 chemical transport models (CTMs). The study focused on air pollution issues related to sulphur
66 (S) (including SO₂, SO₄²⁻ and wet SO₄²⁻ deposition). The second phase of MICS-Asia (MICS-Asia

67 II) was launched in early 2000s with nine CTMs (Carmichael and Ueda, 2008). The study covered
68 the chemistry and transport of S, nitrogen (N), PM and acid deposition. Multi-model results on
69 SO_4^{2-} , NO_3^- and NH_4^+ (SNA) were evaluated with measurements from fourteen sites of Acid
70 Deposition Monitoring Network in East Asia (EANET) and the Fukue site in Japan. However, a
71 non-exhaustive evaluation on PM_{10} concentrations in China with scarce datasets left an unclear
72 view of models' ability in this area, a region recognized as one of the most heavily polluted in EA.
73 Meanwhile, model results were found with high inconsistencies on simulating both gas and aerosol
74 phases of S and N (Hayami et al., 2008). Further efforts are needed to investigate the reasons for
75 model differences to improve model accuracies.

76 This study compares the performances of twelve regional models participated in the third
77 phase of MICS-Asia (MICS-Asia III) on simulating PM over EA. The comparison among models
78 aims at identifying the reasons for different model performances. The models involved in this
79 study include Weather Research and Forecasting Model (WRF) coupled with Community
80 Multiscale Air Quality Modeling (CMAQ) (version 4.7.1 and v5.0.2), WRF model coupled with
81 Chemistry (WRF-Chem) (v3.6.1 and v3.7.1), Goddard Earth Observing System coupled with
82 Chemistry (GEOS-Chem), Non-Hydrostatic Model coupled with Chemistry (NHM-Chem),
83 Nested Air Quality Prediction Modeling System (NAQPMS) and NASA-Unified WRF (NU-
84 WRF). The model performance on simulating PM has been reported in a companion paper (Chen
85 et al., 2019). The main findings are described in sect. 3.1. Sections 3.2-3.4 examine the influences
86 of three model processes on model performances: (1) Formation of fine particles (PMF): model
87 differences in the gas-particle conversion. (2) Formation of coarse particles (PMC): model
88 improvements by implementing dust emissions/modules on simulating PM and the remaining
89 problems. (3) Removal processes of particles from the atmosphere: uncertainties lay on the
90 efficiencies of wet and dry depositions. Section 4 concludes the findings of this study and provides
91 suggestion for further study.

92 **2 Methodology**

93 **2.1 Framework of MICS-Asia**

94 MICS-Asia is a model intercomparison study with contributions from international modelling
95 groups to simulate the air quality and deposition over EA. MICS-Asia I focused on air quality
96 issues related to S. The multi-model performances on simulating SO_2 and SO_4^{2-} concentrations and

97 SO₄²⁻ wet deposition were evaluated with observation from eighteen stations (Carmichael et al.,
98 2002). A source-receptor relationship of S deposition was developed based on the sensitivity
99 simulations for seven prescribed receptor regions: Komae, Oki, Fukue, Yangyang, Beijing,
100 Nanjing and Taichung (Carmichael et al., 2002).

101 MICS-Asia II was initiated in 2003. Nine regional models simulated the air qualities for
102 four months (March, July and December of 2001 and March of 2002) to study the chemistry and
103 transport of air pollutants and acid deposition (Carmichael and Ueda, 2008). All modelling groups
104 were enforced to use the same emission: the Transport and chemical Evolution over the Pacific
105 (TRACE-P) emission of 2000, and common IC/BC to facilitate a comparison on the physical and
106 chemical mechanisms of models. The modelling species expanded to S, N, O₃, PM and acid
107 deposition. Model evaluations and major findings can be found in literature (Carmichael et al.,
108 2008;Fu et al., 2008;Han et al., 2008;Hayami et al., 2008).

109 MICS-Asia III is launched in 2010. The simulation time covers the whole year of 2010.
110 All modelling groups are required to use the prescribed anthropogenic and natural inputs (Li et al.,
111 2017). Three purposes are set for this project– topic I: evaluating the strengths and weaknesses of
112 current multi-scale air quality models in simulating air qualities over EA and providing suggestion
113 to reduce uncertainty for future simulations, topic II: developing a reliable anthropogenic emission
114 inventory for EA, topic III: investigating the interaction of aerosol-weather-climate by using online
115 coupled air quality models. This study focuses on topic I.

116

117 **2.2 Model configurations**

118 The model set-up can be found in Table 1 of Chen et al. (2019). Fourteen modeling groups (M1-
119 M14) participated, but M3 and M9 are not included in this study due to uncompleted model
120 submission. M14 model has a smaller simulation domain than the others, therefore it is not
121 included in the multi-model mean (MMM) results. The gas and aerosol modules and dust schemes
122 employed by the participating models were introduced in detail in sector 2.1 of Chen et al., 2019.
123 Following are the descriptions on the model set-up for wet and dry deposition.

124 Wet deposition removes gases and aerosols from the atmosphere by rain droplets, involving
125 both in-cloud scavenging (rainout) and below-cloud scavenging (washout). The gases in the

126 atmosphere are dissolved in the raindrop and then removed from the atmosphere. For the non-
127 reactive gases, the removal rate depends on the solubility of gases and is a function of the Henry's
128 Law. Particles participate in the cloud condensation nuclei in the presence of supersaturation water
129 vapor and then grow into cloud droplets. In this study, only M2, M4, M6, M11 and M12 have
130 submitted the main components of S and N depositions. All these models use the same wet
131 deposition scheme based on Henry's law. The efficiency of wet deposition is assessed by the so-
132 called "washout ratio", calculated as the ratio of particle concentrations in deposition to particle
133 concentrations in surface air as shown in Eq. 1.

$$134 \quad \lambda_{wet} = \frac{C_{depo}}{C_{surface_air}} \times 100\% \quad (1)$$

135 where λ_{wet} is the washout ratio for wet deposition, C_{depo} is the concentration of particles in
136 deposition and $C_{surface_air}$ is the concentration of particles at near surface atmosphere.

137 Dry deposition is mainly driven by turbulent and molecular diffusion processes. All models
138 except M12 use the same dry deposition scheme from Wesely (1989). The dry deposition flux is
139 proportional to the concentration of pollutants at height. The dry deposition velocity is calculated
140 with Eq. 2.

$$141 \quad V_d = -F_c / C_a \quad (2)$$

$$142 \quad V_d = \frac{1.0}{r_{surf} + r_a + r_{bc}} \quad (3)$$

143 where F_c is the dry deposition flux, V_d is the deposition velocity and C_a is the concentration of
144 species at height. The negative mark indicates the direction of the dry deposition velocity. The V_d
145 is determined by the resistance of air layer (r). The total r is composed of three factors (Eq. 3): the
146 aerodynamic resistance (r_a), boundary layer resistance (r_{bc}) and canopy resistance (r_{surf}).

147 M12 uses the general approach from Wesely (1989) and updates by Zhang et al. (2003).
148 Zhang et al. (2003) updates the value of non-stomatal resistance (R_{ns}), which is a component of
149 R_{surf} related to the soil uptake and cuticle uptake of dry deposition. Model evaluation shows the
150 updates can improve the model prediction on dry deposition velocities of SO_2 (Zhang et al., 2003).

151

152 **2.3 Observation data**

153 To make the discussion clear, we define the regions used in the following analysis here: northern
154 EA (Russia and Mongolia), central EA (China), western EA (Japan and Korea) and southern EA
155 (Cambodia, Lao PDR, Myanmar, Thailand, Vietnam, Indonesia, Malaysia and Philippines).
156 Following monitoring datasets are used in the analysis in sects. 3.2-3.4: Air Pollution Indices
157 (APIs) provides monthly average PM_{10} data from eighty-six sites (A1-A86 in Fig 1)
158 (<http://datacenter.mep.gov.cn/>). This dataset has been widely used to study the PM pollution (Qu
159 et al., 2010;Chen et al., 2008;Deng et al., 2011) as well as model evaluation (Wang et al.,
160 2012;Xing et al., 2015) in China. It is replaced by the Air Quality Index (AQI) after 2013. The
161 APIs data covers the eastern China well with intensively located sites, but sites in western China
162 are very limited. EANET (E1-E54) provides monthly average concentrations of PM_{10} , SNA and S
163 and N depositions from fifty-four sites (<http://www.eanet.asia/>, last access: 28 May 2018). For
164 PM_{10} , this dataset has very limited number of sites in China. The sites are generally located along
165 the east coast of China and couldn't well cover the areas with high PM_{10} pollution, such as the
166 Hebei-Beijing-Tianjin (HBT) region (Fig. 1). And the data completeness in northern EA is not as
167 satisfied as the other regions. Only three sites located in Rishiri (E15), Ochiishi (E16) and Oki
168 (E21) in Japan have $PM_{2.5}$ observation during our study period. R1-R35 (green) are thirty-five
169 Reference (Ref) sites provided by the Institute of Atmospheric Physics Chinese Academy of
170 Science (IAP_CAS). The sites are intensively located in three regions: HBT region, Pearl River
171 Delta (PRD) and Taiwan.

172

173 **3 Result and discussion**

174 **3.1 Brief results of model performance evaluation**

175 All models have submitted the monthly average concentrations of PM_{10} , $PM_{2.5}$ and SNA at surface
176 layer except PM_{10} from M13 and NO_3^- and NH_4^+ from M10. Evaluation of model performance on
177 aerosols can be found in our companion paper (Chen et al., 2019). Following are the main findings:
178 PM_{10} concentrations were generally underestimated over the simulation domain. $PM_{2.5}$
179 concentrations were also underestimated over Eastern EA, but were well simulated in Central EA.
180 Models failed to reproduce the high peaks of SO_4^{2-} concentration in Central EA, probably due to

181 missing SO_4^{2-} formation mechanisms (such as heterogeneous SO_4^{2-} chemistry), which has been
182 reported as an important formation pathway of SO_4^{2-} in China. NO_3^- concentrations were
183 overpredicted by most models over the simulation domain and were associated with the
184 underestimation of SO_4^{2-} . M7 and M8 models produced significantly lower NO_3^- concentrations
185 than observations and other models, due to model bias in simulating the NH_3 concentrations and
186 missing the N_2O_5 heterogeneous reaction that serves as an important formation pathway of NO_3^- . The
187 spatial distributions of AOD were generally well simulated except the underestimation around the
188 Himalaya mountains, Taklamakan Desert and Gobi Desert.

189 This study compares the model performances with global-scale model study. The Task
190 Force on Hemispheric Transport of Air Pollution (TF HTAP) is an inter-comparison study of
191 global and regional models to assess the impact of hemispheric transport of air pollutants on
192 regional atmosphere. The second phase of HTAP (HTAP-II) involved more than twenty global
193 models to simulate the air quality in 2010 (Galmarini et al., 2017). Most models utilize coarse-
194 resolution grids at about 2° - 3° . The HTAP-II and MICS-Asia III share some common points like
195 using the same emission inventory in East Asia (Li et al., 2017) and using the same observation
196 dataset to evaluate PM_{10} (more than 100 EANET and API sites) and $\text{PM}_{2.5}$ (two EANET sites)
197 (Dong et al., 2018). The mean bias (MB) of PM_{10} over EA is $-30.7 \mu\text{g m}^{-3}$ and $-18.6 \mu\text{g m}^{-3}$ for
198 HTAP-II and this study, respectively (values for sites used by both studies). And the MB of $\text{PM}_{2.5}$
199 is $-1.6 \mu\text{g m}^{-3}$ and $-4.3 \mu\text{g m}^{-3}$ for HTAP-II and this study, respectively. Both studies find
200 underestimation of PM_{10} concentrations, while $\text{PM}_{2.5}$ concentrations are well produced. Models of
201 MICS-Asia III perform slightly better than those of HTAP-II with lower model bias in PM_{10} ,
202 probably taking the advantage of finer resolutions of model grids.

203 The so-called “diagnostic evaluation” approach is adopted to check the model bias oriented
204 by individual process (Dennis et al., 2010). Although all modelling groups are required to use the
205 prescribed emission inventory, but mismatch was found during the temporal and vertical
206 treatments of emission files by different modelling groups and has caused differences in the model
207 inputs (Itahashi et al., 2019). To avoid the possible impacts on inter-model comparison, we
208 compare the indicators (i.e. sulphur oxidation ratio (SOR)) instead of direct model outputs (i.e.
209 SO_4^{2-} concentrations) to focus on the differences caused by model mechanisms. The following
210 three processes are examined:

- 211 (1) Formation of PMF: sect. 3.2 investigates the differences in the gas-particle conversion of S
 212 and N among different models.
- 213 (2) Formation of PMC: sect. 3.3 assesses the model abilities in reproducing the spatial and
 214 temporal distributions of PM in regions affected by dust storm. A comparison is conducted
 215 between models with and without dust emissions/modules.
- 216 (3) Removal of particles from the atmosphere: sect. 3.4 compares the model performances in
 217 simulating the amounts of deposition and the efficiencies of wet and dry depositions.

218

219 3.2 Gas-particle conversion

220 The following two indicators are calculated to illustrate the gas-particle conversions of S and N.

$$221 \quad SOR = \frac{n-SO_4^{2-}}{n-SO_4^{2-} + n-SO_2} \quad (4)$$

$$222 \quad C(NO_2) = \frac{n-NO_3^-}{n-NO_3^- + n-NO_2} \quad (5)$$

223 where $n-SO_4^{2-}$, $n-SO_2$, $n-NO_3^-$ and $n-NO_2$ are the mole concentrations of SO_4^{2-} particle, SO_2 gas,
 224 NO_3^- particle and NO_2 gas. The $C(NO_2)$ indicator only has NO_3^- and NO_2 in the denominator due
 225 to the limitation of observation data. But it still can portrait the conversion of N between gas phase
 226 and particle phase.

227 Figures 2 and 3 show the distributions of SOR and $C(NO_2)$ values of models. The SOR
 228 values are lowest around the HBT region in north-eastern China (10-40%) and highest in south-
 229 western China (60-80%) (Fig. 2). The X-CMAQ models (including WRF-CMAQ and RAMS-
 230 CMAQ) produce similar SOR patterns, except that the CMAQv5.0.2 models (M1 and M2) predict
 231 10% higher SOR in the HBT region than the CMAQv4.7.1 models (M4, M5 and M6). CMAQv502
 232 updated the production of SO_4^{2-} in the aqueous reaction of the older version (Appel et al., 2013;
 233 Fountoukis and Nenes, 2007). The explicit treatment of Fe and Mn allows more consistent
 234 treatment of aqueous reaction from SO_2 to SO_4^{2-} . For the X-Chem models (including WRF-Chem,
 235 GEOS-Chem and NHM-Chem), the two WRF-Chem models (M7 and M8) produce similar
 236 magnitudes and distributions of SOR in all regions, except the south-western China (around Tibet
 237 in Fig. 1) and the open oceans, while the NHM-Chem (M12) and GEOS-Chem (M13) models
 238 produce slightly higher SOR values over the whole simulation domain. The differences between

239 the X-CMAQ and the X-Chem models are significant over the inland regions of northern and
240 eastern China, Japan and southern EA. The X-CMAQ models generally predict 5-20% higher *SOR*
241 values than the X-Chem models. Similarly, the X-CMAQ models generally give 20% higher
242 $C(NO_2)$ values than the WRF-Chem models, especially in eastern EA (Fig. 3). The $C(NO_2)$ of M8
243 is extremely low due to unreasonably low NO_3^- concentrations.

244 Figure 4 shows the gas-particle conversions of S and N by models and observation at the
245 EANET sites. The red bars represent concentrations of gases and the black bars represent
246 concentrations of aerosols. The values with blue color above the bars are observed and modelled
247 *SOR* and $C(NO_2)$ values. Results for individual sites are available in supplementary Fig. S1.
248 According to Fig. 4(a), the total amount of S (SO_2 gas+ SO_4^{2-} particle) is about $0.15 \mu\text{mole(S)} \text{ m}^{-3}$.
249 Most models have biases on this value, especially the moderate underestimation by M7, M8 and
250 M13. On the other hand, the *SOR* value (0.25) is well simulated by M1 (0.26), M2 (0.20), M10
251 (0.29) and M13 (0.26). Other models generally under-predict the *SOR* value except M12 (0.33)
252 and M14 (0.57). The WRF-CMAQv5.0.2 models (M1 and M2) produce higher *SOR* than WRF-
253 CMAQv4.7.1 models (M4, M5 and M6), probably attributed to the updates in the formation
254 pathway of SO_4^{2-} .

255 Figure 4(b-e) show the results in different regions. In northern EA, the total amount of S is
256 underestimated by all models except M13 and M14. However, the *SOR* value (0.12) is well
257 reproduced by most models (0.08-0.20) except M12 (0.25) and M10 (0.32). There is only one site
258 available for central EA. Most models (except M12 and M13) have largely underestimated the
259 *SOR* value, while M14 has largely overestimated it. For eastern EA, the total amount of S is well
260 captured by all models except M11, M12 and M14. The *SOR* value (0.55) is generally
261 underestimated by all models except M10 (0.55) and M14 (0.71). For southern EA, the total
262 amount of S is generally overestimated by all models except M13, while the *SOR* value is
263 underestimated by all models except M13 and M14. Overall, the models have both positive and
264 negative biases in simulating the total amounts of S, but generally underestimated the *SOR* values
265 in all regions. Furthermore, the modelled *SOR* values vary largely among models (ranging from
266 0.12 to 0.57), resulting in a large inter-model difference (1sd% = 50%). This variation is of the
267 same magnitude as the variation of SO_4^{2-} concentration (1sd% = 50% in supplementary Fig. S2).

268 The results suggest that differences in gas-particle conversion among models could account largely
269 for the models' inconsistency in simulating the SO_4^{2-} concentrations.

270 Figure 4(f-h) compares the gas-particle conversion of N with the $C(\text{NO}_2)$ indicator. Only
271 one site in China and one site in Japan have both NO_2 and NO_3^- observations. At the Hongwen
272 sites in China, all models except M5 underestimate the sum of NO_2 and NO_3^- , but the modelled
273 $C(\text{NO}_2)$ values are close to the observation (0.18) except M5 (0.07), M8 (0.00) and M12 (0.40).
274 Similar to the results of S conversion, the newer version of WRF-CMAQ model generally produces
275 higher $C(\text{NO}_2)$ than the older version, but the differences between the two are smaller. At the
276 Banryu site in Japan, the sum of NO_2 and NO_3^- is well simulated by all models except M8. The
277 $C(\text{NO}_2)$ (0.19) value is also well simulated by all models except M8 (0.00), M12 (0.53) and M14
278 (0.77). Overall, the model accuracy on $C(\text{NO}_2)$ is slightly higher than that on SOR according to the
279 comparison with observed values. Models also have higher consistencies on $C(\text{NO}_2)$ than SOR .
280 However, further validation is required due to the limited number of observations for the
281 conversion of N.

282

283 **3.3 Implementation of dust emissions/modules in models**

284 The PMC concentrations at surface layer are calculated by subtracting $\text{PM}_{2.5}$ from PM_{10} . Figure 5
285 shows the spatial distribution of annual average PMC of models. Most models show very low ($<$
286 $2\mu\text{g m}^{-3}$) concentrations of PMC around the Takalmakan Desert and the Gobi Desert in northern
287 China except M10, M11 and M14. These three models use dust emissions/modules in simulations
288 (Chen et al., 2019). M12 also includes dust emissions, but its PM_{10} concentrations over northern
289 China are much lower than the three models. The predicted PMC concentrations of the three
290 models differ largely. The domain-average concentrations of PMC are 21, 7 and $12\mu\text{g m}^{-3}$ for
291 M10, M11 and M14, respectively. The distributions of PMC also differ largely over north-west
292 China, where the impacts of dust are most significant. The differences among the models mainly
293 comes from the different parameterizations such as source functions, dust-lifting mechanisms and
294 size distributions of particles (Chen et al., 2019). Different PMC concentrations are also found
295 over oceans, mainly attributed to the sea-salt emissions in this study. The sea-salt emissions are
296 parameterized in the models with various formula (Chen et al., 2019). In this study, the WRF-
297 Chem models (M7 and M8) do not account for sea-salt emissions, thus their PMC concentrations

298 over the oceans and seas are not defined. The two WRF-CMAQ models use the in-line sea-salt
299 emission module of Gong (2003) and updated by Kelly et al. (2010). They predict consistent
300 distributions of PMC over oceans. M10 and M11 use the same module as the CMAQ models
301 (Gong, 2003), but produce higher PMC on oceans. M12 adopts the method of breaking wave over
302 seashore by Clarke et al. (2006) and produces the highest PMC over oceans among all models.

303 The implementation of dust emission is expected to improve the model performances, but
304 how significant could the improvement be? And can models predict the PM concentrations
305 reasonably at regions affected by dust with current dust emissions/modules? To answer these
306 questions, all sites are grouped to dust and non-dust sites according to their locations. The sites
307 located in regions that have been reported to receive severe impacts and rapid deposition of dust
308 are marked as dust sites (Shao and Dong, 2006) (grey-color shaded areas in Fig. 1). Figure 6(a-b)
309 and Table 1 compare the model performances at the dust and non-dust sites. For the non-dust sites
310 (Fig. 6(b)), most models have well captured the magnitudes of PM_{10} at the “API non-coastal, non-
311 dust” sites (MB = -8% and NMB = -8%). The sites marked as “API coastal” sites, which are located
312 close to the coastal regions, are all slightly underestimated by about $25 \mu\text{g m}^{-3}$ (30%). Similarly,
313 the PRD and Taiwan sites, which are also located near the coastal regions, are all underestimated
314 by about $20 \mu\text{g m}^{-3}$ (37%). Bias in sea-salt emissions is the possible reason. Sea-salt emission is
315 reported to contribute to 20-40% of SNA and PM_{10} over coastal regions (Liu et al., 2015).
316 Including the sea-salt emission in model simulation can improve the model accuracy with 8-20%
317 increase in PM_{10} , SNA, Na^+ and Cl^- (Kelly et al., 2010;Im, 2013). The influence of sea-salt
318 emission is not the focus of this study, but further study is strongly recommended.

319 For the dust sites (Fig. 6(a)), most models have generally underestimated the PM_{10}
320 concentrations by $10\text{-}40 \mu\text{g m}^{-3}$ (15-50%). And the three models with dust module perform better
321 than the others at the dust sites, especially site A2, A30, A68, A69, R5 and R18. However, they
322 miss the high PM_{10} concentrations at sites like R1-R3 and R11, and overestimate the PM_{10}
323 concentrations at sites such as A60 and A80. This indicates that the dust emissions/modules
324 involved in this study can't fully capture the magnitudes and distributions of dust pollutions over
325 EA. In addition, the modelled PMC differ a lot with different dust emissions/modules (Fig. 5).
326 M10 model produces very high PMC over the whole eastern China, while M11 model only predicts
327 high PMC around the HBT region. Overall, the model performance on PM over dust regions can

328 be improved largely by including dust emissions/modules. However, the concentrations and
329 distributions are not yet well captured and large inconsistencies are found among different dust
330 emissions/modules.

331 Figure 6(c-d) compares the modelled monthly trends of PM₁₀ with observations at the dust
332 and non-dust sites and Fig. 6(e) shows the correlations (R) values between models and observation.
333 For the non-dust sites (Fig. 6(d)), the trends are well caught by most models. The R values are
334 close to 0.70 for all models except M7 (0.62), M8 (0.58) and M14 (0.63). The WRF-Chem models
335 (M7 and M8) simulate too low PM₁₀ concentrations in winter. M14 model overestimates the PM₁₀
336 concentrations during March to May. Most models have much lower R values at the dust sites than
337 the non-dust sites (Fig. 6(e)), due to underestimation of the PM₁₀ concentrations during winter.
338 For instance, R values of M10 drop from 0.7 at the non-dust sites to 0.11 at the dust sites. Spring
339 (March, April and May) has the largest model biases at the dust sites, which is coincident with the
340 dust storm season in Asia (Arimoto et al., 2006). M10 and M14 models perform well in most
341 months at both the dust and non-dust sites, taking the advantage of their dust emissions/modules.
342 But their R values at the dust sites are very low. Future study is strongly suggested on a better
343 understanding of the seasonal variations of dust pollutions.

344 **3.4 Wet and dry depositions**

345 Figure 7 and Table 2 show the model performance on wet deposition. For wet SO₄²⁻ deposition,
346 despite that the two sites with highest deposition (E2 and E3) in China are underestimated, the
347 other sites are generally well simulated by MMM with a low MB of -8%. The individual model
348 bias varies from -22% to 41%. The CMAQ models (M2, M4 and M6) all underestimate the wet
349 SO₄²⁻ deposition. There are large differences between CMAQv4.7.1 and CMAQv5.0.2 in JP,
350 where the CMAQv4.7.1 models (M4 and M6) slightly overestimate the wet SO₄²⁻ deposition at
351 E19 and E23, while the CMAQv5.0.2 model (M2) slightly underestimates the value at these sites.
352 The M11 model produces considerably higher wet deposition of SO₄²⁻ and NO₃⁻ than the other
353 models in East EA. The possible reasons are discussed later. The MMM underestimates the NO₃⁻
354 wet deposition by 29%, due to large under-prediction in southern EA. The southern EA has several
355 sites with very high deposition, such as E29 site in MY and E35 and E36 sites in PH, but all models
356 fail to catch those high peaks. The individual model bias varies from -59% to 30% among models.
357 M2, M4, M6 and M12 perform similarly with high underestimation ranging from 39% to 59%.

358 The M11 is the only model that succeeded to capture the high wet NO_3^- deposition at E2 and E3 in
359 CH, but it overestimates most sites in CH, JP and KR. In case of wet NH_4^+ deposition, the MMM
360 generally underestimates the amount at all sites with a bias of -40%, especially at E2-E4 in CH,
361 E45 in TH and E35 and E36 in PH. The individual model bias varies from -10% to -37%. The M2,
362 M4 and M6 models perform similarly, while M11 and M12 models predict higher depositions at
363 all sites. Overall, large inter-model disagreements are found in eastern EA for wet deposition of
364 SO_4^{2-} and NO_3^- and in southern EA for the wet NH_4^+ deposition. The observation of dry deposition
365 is composed by observed concentration of air pollutants and simulated deposition velocity. Since
366 the EANET network only provides the former one, complete evaluation of the dry deposition is
367 not available in this study (complete dry deposition with velocity is available after 2013).

368 Table 3 lists the domain-total annual-accumulated amounts of S and N depositions by
369 models. The total wet S deposition (D_{Swet}) includes wet depositions of SO_2 , H_2SO_4 and SO_4^{2-} . The
370 total dry S deposition (D_{Sdry}) includes dry deposition of SO_2 , H_2SO_4 and SO_4^{2-} . The total wet N
371 deposition (D_{Nwet}) includes wet depositions of NO_3^- , NH_4^+ , HNO_3 , NH_3 . The total dry N
372 depositions (D_{Ndry}) includes dry deposition of NO , NO_2 , NO_3^- , NH_4^+ , HNO_3 and NH_3 . D_{Swet} values
373 range from 10.5 to 31.3 Tg(S) yr^{-1} among models (1sd%=75%). The estimation by M11 model is
374 two folds higher than the other four models. The inter-model difference is significant even among
375 the same type of models with different versions. The CMAQv4.7.1 models (M4 and M6) produce
376 12.5 Tg(S) yr^{-1} (M4) and 13.8 Tg(S) yr^{-1} (M6) of D_{Swet} , while the prediction by CMAQv5.0.2
377 model (M2) is 25% lower. Despite the large discrepancies in the total amount, all five models
378 agree that over 95% of D_{Swet} is wet SO_4^{2-} deposition. The total amounts of D_{Sdry} range from 4.3 to
379 10.6 Tg(S) yr^{-1} among models (1sd% =39%). M11 predicts higher D_{Sdry} than other models and the
380 CMAQv5.0.2 model (M2) predicts 45% lower D_{Sdry} than the two CMAQv4.7.1 models (M4 and
381 M6). Similar to D_{Swet} , all models have high agreements on the proportions of the components.
382 D_{Nwet} range from 12.2 to 20.0 Tg(N) yr^{-1} among models (1sd%=21%). The CMAQ models (M2,
383 M4 and M6) simulate close results (12-15 Tg(N) yr^{-1}), while M11 (20.0 Tg(N) yr^{-1}) and M12 (16.5
384 Tg(N) yr^{-1}) simulate slightly higher amounts. As for the proportion of components, M2, M4, M6
385 and M12 models predict high proportions of wet NO_3^- and wet NH_4^+ depositions (particle phase),
386 while M11 model produces higher percentages of wet HNO_3 and wet NH_3 depositions (gas phase).
387 D_{Ndry} range from 3.9 to 14.1 Tg(N) yr^{-1} (1sd%=38%). M12 gives a considerably lower amount
388 than the other models. Models are quite consistent on the proportions of components.

389 Figure 8(a-e) show λ_{wet} of S deposition ($\lambda_{S_{wet}}$) by models. The CMAQ models (M2, M4 and
390 M6) have similar patterns in $\lambda_{S_{wet}}$ over the inland regions, while M12 model predicts 30-90% lower
391 ratios in India. M11 model generally predicts about 20-70% lower $\lambda_{S_{wet}}$ than the other four models
392 except India, where the difference could reach upmost 170%. For λ_{wet} of N deposition ($\lambda_{N_{wet}}$) (Fig.
393 8(f-j)), the CMAQv4.7.1 models (M4 and M6) and M12 perform similarly, but the CMAQv5.0.2
394 model (M2) predicts 30% lower $\lambda_{N_{wet}}$ in India, Japan and Korea. M11 generally predicts lower
395 ratios in India (60% lower), Indonesia and Philippines (120% lower) than the CMAQ models.
396 Figure 9 shows the spatial distributions of V_d . For V_d of S deposition (V_{S_d}) (Fig. 9(a-e)), the CMAQ
397 models (M2, M4 and M6) simulate very similar spatial distributions. M11 and M12 models predict
398 0.5 cm s^{-1} lower V_{S_d} than the CMAQ models over the whole inland regions, especially in east China
399 and India peninsular. For V_d of N deposition (V_{N_d}) (Fig. 9(f-j)), the CMAQ models (M2, M4 and
400 M6) predict very similar distributions. M11 and M12 predict about 0.3 cm s^{-1} and $1-2 \text{ cm s}^{-1}$ lower
401 V_{N_d} than the CMAQ models over the inland regions. Both λ_{wet} and V_d of M11 are much lower than
402 the other models, especially over eastern EA. And this is a possible reason for the biased
403 performance of M11 on wet deposition (Fig. 7). Overall, large inter-model differences are found
404 in predicting both the amounts of depositions and the efficiencies of depositions.

405

406 **4 Conclusion**

407 The topic I of the MICS-Asia III aims at (i) evaluating the strengths and weaknesses of current
408 multiscale air quality models in simulating concentration and deposition fields over East Asia and
409 (ii) providing suggestions for future model developments. This study compares the performances
410 of twelve regional models for the prediction of PM concentrations over EA. The participating
411 models includes WRF-CMAQ (v4.7.1 and v5.0.2), WRF-Chem (v3.6.1 and v3.7.1), GEOS-Chem,
412 NHM-Chem, NAQPMS and NU-WRF. Three processes/mechanisms are investigated to identify
413 the causes of inter-model differences:

414 (1) For the formations of PMF, SOR and $C(NO_2)$ values are used to demonstrate the inter-model
415 differences in gas-particle conversions. The SOR values are generally underestimated by most
416 models at the EANET sites. A generally trend is found that the WRF-CMAQv5.0.2 models
417 produce the highest SOR values among all models, followed by the WRF-CMAQv4.7.1 models
418 (10% lower in HBT region), the WRF-Chem models and other models (5-20% lower over

419 inland regions). The inter-model variation on *SOR* (1sd% =50%) is of the same magnitude as
420 that on SO_4^{2-} concentration. Similar results are found in $C(\text{NO}_2)$, but models have higher
421 agreements on $C(\text{NO}_2)$ than *SOR*. The different treatments of gas-particle conversions account
422 largely for the different model performances on PMF.

423 (2) For the formations of PMC, the models without dust emissions/modules generate very low
424 ($<2\mu\text{g m}^{-3}$) PMC concentrations. They can well capture the PM_{10} concentrations at non-dust-
425 affected sites but underestimate the PM_{10} concentrations at sites affected by dust storms by
426 upmost 50%. This underestimation is largely improved by implementing dust
427 emissions/modules (bias reduced to around -20%). However, both the magnitudes and
428 distributions of dust pollutions are not fully captured. In addition, models employing different
429 dust emissions/modules show large disagreements on the distributions of PMC.

430 (3) For the removal of PM from the atmosphere, the amounts of atmospheric deposition vary
431 largely among models (1sd%) by 75%, 39%, 21% and 38% for D_{Swet} , D_{Sdry} , D_{Nwet} and D_{Ndry} ,
432 respectively. The λ_{wet} and V_d indicators are used to exclude the influences brought by model
433 inputs. For λ_{wet} , models agree more on the D_{Swet} than D_{Nwet} . The largest model inconsistencies
434 are found in India (upmost 170%), Indonesia and Philippines (upmost 120%). For V_d , models
435 differ more on D_{Ndry} than D_{Sdry} , which is opposite to λ_{wet} . The inter-model differences are
436 widely found over the inland regions for D_{Sdry} (about 0.5 cm s^{-1}) and D_{Ndry} ($0.3\text{-}2\text{ cm s}^{-1}$).

437 The main contributions of this study are: (1) comparing the conversions of S and N between gas
438 and particle phases among different models as well as with observations. The comparison with
439 observation makes it possible to both quantify the inter-model differences and tell which module
440 might be more reasonable; (2) Several new updates on dust modules have been published in recent
441 literature, but there is limited study on the inter-comparison. This study provides an opportunity
442 to bring together the new updates on dust modules/emission and review their performance in EA;
443 (3) providing a comprehensive view on the total budget of S and N aerosols, by including the
444 analysis on the removal processes. It turns out that this process brings significant uncertainties to
445 inter-model differences. It should be noted that other factors such as vertical diffusion can also
446 contribute to model differences. Meanwhile, this study focuses on comparing the model abilities
447 in simulating PM in 2010. The chemical regimes may have changed drastically due the rapid
448 changes of emissions and implementation of control policies in Asia. Studies on more recent years
449 and heavily polluted episodes are under preparation.

450

451 *Author Contributions.* JT and JSf designed the study. JT processed and analysed the data. JSF,
452 GRC, SI and ZT contributed to the results and discussions. JSF, ZT, KH, SI, KY, TN, YM, XW,
453 YL, HJL, JEK, CYL, BG, MK, JZ, MZ, LH and ZW provided modelling data. All co-authors
454 provided comments to the manuscript.

455

456 *Data Availability.* The observation data are introduced with details in supplementary sect. S2.1
457 with web links of public available datasets. The model data are available upon request.

458

459 *Competing interests.* The authors declare that they have no conflict of interest.

460 *Acknowledgements.* We thank all participating modeling groups of MICS-Asia III. We
461 acknowledge the support by the Advanced Computing Facility (ACF), Joint Institute for
462 Computational Sciences of the University of Tennessee. We also thank the support by the Oak
463 Ridge National Laboratory for computational resources, which is supported by the Office of
464 Science of the U.S. Department of Energy (contract DE-AC05-00OR22725).

465

466 **Reference**

467 Akimoto, H.: Global air quality and pollution, *Science*, 302, 1716-1719, DOI: 10.1126/science.1092666,
468 2003.

469 Appel, K. W., Pouliot, G. A., Simon, H., Sarwar, G., Pye, H. O. T., Napelenok, S. L., Akhtar, F., and
470 Roselle, S. J.: Evaluation of dust and trace metal estimates from the Community Multiscale Air Quality
471 (CMAQ) model version 5.0, *Geoscientific Model Development*, 6, 883-899, 10.5194/gmd-6-883-2013,
472 2013.

473 Arimoto, R., Kim, Y. J., Kim, Y. P., Quinn, P. K., Bates, T. S., Anderson, T. L., Gong, S., Uno, I., Chin,
474 M., Huebert, B. J., Clarke, A. D., Shinozuka, Y., Weber, R. J., Anderson, J. R., Guazzotti, S. A., Sullivan,
475 R. C., Sodeman, D. A., Prather, K. A., and Sokolik, I. N.: Characterization of Asian Dust during ACE-
476 Asia, *Global Planet Change*, 52, 23-56, <https://doi.org/10.1016/j.gloplacha.2006.02.013>, 2006.

477 Bessagnet, B., Pirovano, G., Mircea, M., Cuvelier, C., Aulinger, A., Calori, G., Ciarelli, G., Manders, A.,
478 Stern, R., Tsyro, S., Vivanco, M. G., Thunis, P., Pay, M. T., Colette, A., Couvidat, F., Meleux, F., Rouil,
479 L., Ung, A., Aksoyoglu, S., Baldasano, J. M., Bieser, J., Briganti, G., Cappelletti, A., D'Isidoro, M.,
480 Finardi, S., Kranenburg, R., Silibello, C., Carnevale, C., Aas, W., Dupont, J. C., Fagerli, H., Gonzalez, L.,
481 Menut, L., Prevot, A. S. H., Roberts, P., and White, L.: Presentation of the EURODELTA III
482 intercomparison exercise - evaluation of the chemistry transport models' performance on criteria
483 pollutants and joint analysis with meteorology, *Atmospheric Chemistry and Physics*, 16, 12667-12701,
484 <https://doi.org/10.5194/acp-16-12667-2016>, 2016.

485 Carmichael, G. R., Calori, G., Hayami, H., Uno, I., Cho, S. Y., Engardt, M., Kim, S. B., Ichikawa, Y.,
486 Ikeda, Y., Woo, J. H., Ueda, H., and Amann, M.: The MICS-Asia study: model intercomparison of long-
487 range transport and sulfur deposition in East Asia, *Atmospheric Environment*, 36, 175-199,
488 [https://doi.org/10.1016/S1352-2310\(01\)00448-4](https://doi.org/10.1016/S1352-2310(01)00448-4), 2002.

489 Carmichael, G. R., Sakurai, T., Streets, D., Hozumi, Y., Ueda, H., Park, S. U., Fung, C., Han, Z., Kajino,
490 M., Engardt, M., Bennet, C., Hayami, H., Sartelet, K., Holloway, T., Wang, Z., Kannari, A., Fu, J.,
491 Matsuda, K., Thongboonchoo, N., and Amann, M.: MICS-Asia II: The model intercomparison study for
492 Asia Phase II methodology and overview of findings, *Atmospheric Environment*, 42, 3468-3490,
493 <http://dx.doi.org/10.1016/j.atmosenv.2007.04.007>, 2008.

494 Carmichael, G. R., and Ueda, H.: MICS-Asia II: The model intercomparison study for Asia phase II,
495 *Atmospheric Environment*, 42, 3465-3467, <http://dx.doi.org/10.1016/j.atmosenv.2007.10.003>, 2008.

496 Chen, L., Gao, Y., Zhang, M., Fu, J. S., Zhu, J., Liao, H., Li, J., Huang, K., Ge, B., Wang, X., Lam, Y. F.,
497 Lin, C.-Y., Itahashi, S., Nagashima, T., Kajino, M., Yamaji, K., Wang, Z., and Kurokawa, J.: MICS-Asia
498 III: multi-model comparison and evaluation of aerosol over East Asia, *Atmos. Chem. Phys.*, 19, 11911–
499 11937, <https://doi.org/10.5194/acp-19-11911-2019>, 2019.

500 Chen, Z. H., Cheng, S. Y., Li, J. B., Guo, X. R., Wang, W. H., and Chen, D. S.: Relationship between
501 atmospheric pollution processes and synoptic pressure patterns in northern China, *Atmospheric*
502 *Environment*, 42, 6078-6087, [10.1016/j.atmosenv.2008.03.043](https://doi.org/10.1016/j.atmosenv.2008.03.043), 2008.

503 Clarke, A. D., Owens, S. R., and Zhou, J. C.: An ultrafine sea-salt flux from breaking waves: Implications
504 for cloud condensation nuclei in the remote marine atmosphere, *J Geophys Res-Atmos*, 111,
505 <https://doi.org/10.1029/2005JD006565>, 2006.

506 Cohen, A. J., Brauer, M., Burnett, R., Anderson, H. R., Frostad, J., Estep, K., Balakrishnan, K.,
507 Brunekreef, B., Dandona, L., Dandona, R., Feigin, V., Freedman, G., Hubbell, B., Jobling, A., Kan, H.,
508 Knibbs, L., Liu, Y., Martin, R., Morawska, L., Pope, C. A., Shin, H., Straif, K., Shaddick, G., Thomas,
509 M., van Dingenen, R., van Donkelaar, A., Vos, T., Murray, C. J. L., and Forouzanfar, M. H.: Estimates
510 and 25-year trends of the global burden of disease attributable to ambient air pollution: an analysis of data
511 from the Global Burden of Diseases Study 2015, *Lancet*, 389, 1907-1918, [10.1016/s0140-](https://doi.org/10.1016/s0140-6736(17)30505-6)
512 [6736\(17\)30505-6](https://doi.org/10.1016/s0140-6736(17)30505-6), 2017.

513 Deng, J. J., Wang, T. J., Jiang, Z. Q., Xie, M., Zhang, R. J., Huang, X. X., and Zhu, J. L.: Characterization
514 of visibility and its affecting factors over Nanjing, China, *Atmospheric Research*, 101, 681-691,
515 [10.1016/j.atmosres.2011.04.016](https://doi.org/10.1016/j.atmosres.2011.04.016), 2011.

516 Dennis, R., Fox, T., Fuentes, M., Gilliland, A., Hanna, S., Hogrefe, C., Irwin, J., Rao, S. T., Scheffe, R.,
517 Schere, K., Steyn, D., and Venkatram, A.: A framework for evaluating regional-scale numerical
518 photochemical modeling systems, *Environ Fluid Mech*, 10, 471-489, doi: 10.1007/s10652-009-9163-2,
519 2010.

520 Dong, X. Y., Fu, J. S., Zhu, Q. Z., Sun, J., Tan, J. N., Keating, T., Sekiya, T., Sudo, K., Emmons, L.,
521 Tilmes, S., Jonson, J. E., Schulz, M., Bian, H. S., Chin, M., Davila, Y., Henze, D., Takemura, T.,
522 Benedictow, A. M. K., and Huang, K.: Long-range transport impacts on surface aerosol concentrations
523 and the contributions to haze events in China: an HTAP2 multi-model study, *Atmospheric Chemistry and*
524 *Physics*, 18, 15581-15600, <https://doi.org/10.5194/acp-18-15581-2018>, 2018.

525 Fountoukis, C., and Nenes, A.: ISORROPIA II: a computationally efficient thermodynamic equilibrium
526 model for K^+ - Ca^{2+} - Mg^{2+} - NH_4^+ - Na^+ - SO_4^{2-} - NO_3^- - Cl^- - H_2O aerosols, *Atmospheric Chemistry and*
527 *Physics*, 7, 4639-4659, <https://doi.org/10.5194/acp-7-4639-2007>, 2007.

528 Fu, J. S., Jang, C. J., Streets, D. G., Li, Z., Kwok, R., Park, R., and Han, Z.: MICS-Asia II: Modeling
529 gaseous pollutants and evaluating an advanced modeling system over East Asia, *Atmospheric*
530 *Environment*, 42, 3571-3583, <http://dx.doi.org/10.1016/j.atmosenv.2007.07.058>, 2008.

531 Fuzzi, S., Baltensperger, U., Carslaw, K., Decesari, S., van Der Gon, H. D., Facchini, M. C., Fowler, D.,
532 Koren, I., Langford, B., Lohmann, U., Nemitz, E., Pandis, S., Riipinen, I., Rudich, Y., Schaap, M.,
533 Slowik, J. G., Spracklen, D. V., Vignati, E., Wild, M., Williams, M., and Gilardoni, S.: Particulate matter,
534 air quality and climate: lessons learned and future needs, *Atmospheric Chemistry and Physics*, 15, 8217-
535 8299, <https://doi.org/10.5194/acp-15-8217-2015>, 2015.

536 Galmarini, S., Koffi, B., Solazzo, E., Keating, T., Hogrefe, C., Schulz, M., Benedictow, A., Griesfeller, J.
537 J., Janssens-Maenhout, G., Carmichael, G., Fu, J., and Dentener, F.: Technical note: Coordination and
538 harmonization of the multi-scale, multi-model activities HTAP2, AQMEII3, and MICS-Asia3:
539 simulations, emission inventories, boundary conditions, and model output formats, *Atmos. Chem. Phys.*,
540 17, 1543-1555, [10.5194/acp-17-1543-2017](https://doi.org/10.5194/acp-17-1543-2017), 2017.

541 Gong, S. L.: A parameterization of sea-salt aerosol source function for sub- and super-micron particles,
542 *Global Biogeochem Cy*, 17, <https://doi.org/10.1029/2003GB002079>, 2003.

543 Han, Z., Sakurai, T., Ueda, H., Carmichael, G. R., Streets, D., Hayami, H., Wang, Z., Holloway, T.,
544 Engardt, M., Hozumi, Y., Park, S. U., Kajino, M., Sartelet, K., Fung, C., Bennet, C., Thongboonchoo, N.,
545 Tang, Y., Chang, A., Matsuda, K., and Amann, M.: MICS-Asia II: Model intercomparison and evaluation
546 of ozone and relevant species, *Atmospheric Environment*, 42, 3491-3509,
547 <http://dx.doi.org/10.1016/j.atmosenv.2007.07.031>, 2008.

548 Hayami, H., Sakurai, T., Han, Z., Ueda, H., Carmichael, G. R., Streets, D., Holloway, T., Wang, Z.,
549 Thongboonchoo, N., Engardt, M., Bennet, C., Fung, C., Chang, A., Park, S. U., Kajino, M., Sartelet, K.,
550 Matsuda, K., and Amann, M.: MICS-Asia II: Model intercomparison and evaluation of particulate sulfate,
551 nitrate and ammonium, *Atmospheric Environment*, 42, 3510-3527,
552 <http://dx.doi.org/10.1016/j.atmosenv.2007.08.057>, 2008.

553 Hoek, G., and Raaschou-Nielsen, O.: Impact of fine particles in ambient air on lung cancer, *Chinese*
554 *Journal of Cancer*, 33, 197-203, [10.5732/cjc.014.10039](https://doi.org/10.5732/cjc.014.10039), 2014.

555 Im, U.: Impact of sea-salt emissions on the model performance and aerosol chemical composition and
556 deposition in the East Mediterranean coastal regions, *Atmospheric Environment*, 75, 329-340,
557 <https://doi.org/10.1016/j.atmosenv.2013.04.034>, 2013.

558 Itahashi, S., Ge, B., Sato, K., Fu, J. S., Wang, X., Yamaji, K., Nagashima, T., Li, J., Kajino, M., Liao, H.,
559 Zhang, M., Wang, Z., Li, M., Kurokawa, J., Carmichael, G. R., and Wang, Z.: MICS-Asia III: Overview
560 of model inter-comparison and evaluation of acid deposition over Asia, *Atmos. Chem. Phys. Discuss.*,
561 <https://doi.org/10.5194/acp-2019-624>, accepted, 2019

562 Kelly, J. T., Bhave, P. V., Nolte, C. G., Shankar, U., and Foley, K. M.: Simulating emission and chemical
563 evolution of coarse sea-salt particles in the Community Multiscale Air Quality (CMAQ) model,
564 *Geoscientific Model Development*, 3, 257-273, <https://doi.org/10.5194/gmd-3-257-2010>, 2010.

565 Knol, A. B., de Hartog, J. J., Boogaard, H., Slottje, P., van der Sluijs, J. P., Lebret, E., Cassee, F. R.,
566 Wardekker, A., Ayres, J. G., Borm, P. J., Brunekreef, B., Donaldson, K., Forastiere, F., Holgate, S. T.,
567 Kreyling, W. G., Nemery, B., Pekkanen, J., Stone, V., Wichmann, H. E., and Hoek, G.: Expert elicitation
568 on ultrafine particles: likelihood of health effects and causal pathways, *Particle and Fibre Toxicology*, 6,
569 10.1186/1743-8977-6-19, 2009.

570 Lamarque, J. F., Shindell, D. T., Josse, B., Young, P. J., Cionni, I., Eyring, V., Bergmann, D., Cameron-
571 Smith, P., Collins, W. J., Doherty, R., Dalsoren, S., Faluvegi, G., Folberth, G., Ghan, S. J., Horowitz, L.
572 W., Lee, Y. H., MacKenzie, I. A., Nagashima, T., Naik, V., Plummer, D., Righi, M., Rumbold, S. T.,
573 Schulz, M., Skeie, R. B., Stevenson, D. S., Strode, S., Sudo, K., Szopa, S., Voulgarakis, A., and Zeng, G.:
574 The Atmospheric Chemistry and Climate Model Intercomparison Project (ACCMIP): overview and
575 description of models, simulations and climate diagnostics, *Geoscientific Model Development*, 6, 179-
576 206, 10.5194/gmd-6-179-2013, 2013.

577 Lelieveld, J., Evans, J. S., Fnais, M., Giannadaki, D., and Pozzer, A.: The contribution of outdoor air
578 pollution sources to premature mortality on a global scale, *Nature*, 525, 367-+, 10.1038/nature15371,
579 2015.

580 Li, J., Wang, Z. F., Zhuang, G., Luo, G., Sun, Y., and Wang, Q.: Mixing of Asian mineral dust with
581 anthropogenic pollutants over East Asia: a model case study of a super-duststorm in March 2010,
582 *Atmospheric Chemistry and Physics*, 12, 7591-7607, DOI: 10.5194/acp-12-7591-2012, 2012.

583 Li, M., Zhang, Q., Kurokawa, J. I., Woo, J. H., He, K., Lu, Z., Ohara, T., Song, Y., Streets, D. G.,
584 Carmichael, G. R., Cheng, Y., Hong, C., Huo, H., Jiang, X., Kang, S., Liu, F., Su, H., and Zheng, B.:
585 MIX: a mosaic Asian anthropogenic emission inventory under the international collaboration framework
586 of the MICS-Asia and HTAP, *Atmos. Chem. Phys.*, 17, 935-963, 10.5194/acp-17-935-2017, 2017.

587 Lippmann, M.: Toxicological and epidemiological studies of cardiovascular effects of ambient air fine
588 particulate matter (PM_{2.5}) and its chemical components: Coherence and public health implications, *Crit
589 Rev Toxicol*, 44, 299-347, DOI: 10.3109/10408444.2013.861796, 2014.

590 Liu, Y. M., Zhang, S. T., Fan, Q., Wu, D., Chan, P. W., Wang, X. M., Fan, S. J., Feng, Y. R., and Hong,
591 Y. Y.: Accessing the Impact of Sea-Salt Emissions on Aerosol Chemical Formation and Deposition over
592 Pearl River Delta, China, *Aerosol Air Qual Res*, 15, 2232-2245, doi: 10.4209/aaqr.2015.02.0127, 2015.

593 Nel, A.: Air pollution-related illness: Effects of particles, *Science*, 308, 804-806, DOI:
594 10.1126/science.1108752, 2005.

595 Qu, W. J., Arimoto, R., Zhang, X. Y., Zhao, C. H., Wang, Y. Q., Sheng, L. F., and Fu, G.: Spatial
596 distribution and interannual variation of surface PM₁₀ concentrations over eighty-six Chinese cities,
597 *Atmospheric Chemistry and Physics*, 10, 5641-5662, 10.5194/acp-10-5641-2010, 2010.

598 Rao, S., Chirkov, V., Dentener, F., Van Dingenen, R., Pachauri, S., Purohit, P., Amann, M., Heyes, C.,
599 Kinney, P., Kolp, P., Klimont, Z., Riahi, K., and Schoepp, W.: Environmental Modeling and Methods for
600 Estimation of the Global Health Impacts of Air Pollution, *Environmental Modeling & Assessment*, 17,
601 613-622, 10.1007/s10666-012-9317-3, 2012.

602 Shao, Y., Dong, C. H. A review on East Asian dust storm climate, modeling and monitoring: *Global and
603 Planetary Change*, 2006, 52(1-4): 1-22.

604 Silva, R. A., West, J. J., Zhang, Y. Q., Anenberg, S. C., Lamarque, J. F., Shindell, D. T., Collins, W. J.,
605 Dalsoren, S., Faluvegi, G., Folberth, G., Horowitz, L. W., Nagashima, T., Naik, V., Rumbold, S., Skeie,

606 R., Sudo, K., Takemura, T., Bergmann, D., Cameron-Smith, P., Cionni, I., Doherty, R. M., Eyring, V.,
607 Josse, B., MacKenzie, I. A., Plummer, D., Righi, M., Stevenson, D. S., Strode, S., Szopa, S., and Zeng,
608 G.: Global premature mortality due to anthropogenic outdoor air pollution and the contribution of past
609 climate change, *Environ Res Lett*, 8, 10.1088/1748-9326/8/3/034005, 2013.

610 Tebaldi, C., and Knutti, R.: The use of the multi-model ensemble in probabilistic climate projections,
611 *Philos T R Soc A*, 365, 2053-2075, <https://doi.org/10.1098/rsta.2007.2076>, 2007.

612 Vivanco, M. G., Bessagnet, B., Cuvelier, C., Theobald, M. R., Tsyro, S., Pirovano, G., Aulinger, A.,
613 Bieser, J., Calori, G., Ciarelli, G., Manders, A., Mircea, M., Aksoyoglu, S., Briganti, G., Cappelletti, A.,
614 Colette, A., Couvidat, F., D'Insidoro, M., Kranenburg, R., Meleux, F., Menut, L., Pay, M. T., Rouil, L.,
615 Silibello, C., Thunis, P., and Ung, A.: Joint analysis of deposition fluxes and atmospheric concentrations
616 of inorganic nitrogen and sulphur compounds predicted by six chemistry transport models in the frame of
617 the EURODELTAIII project, *Atmospheric Environment*, 151, 152-175,
618 <https://doi.org/10.1016/j.atmosenv.2016.11.042>, 2017.

619 Wang, K., Zhang, Y., Nenes, A., and Fountoukis, C.: Implementation of dust emission and chemistry into
620 the Community Multiscale Air Quality modeling system and initial application to an Asian dust storm
621 episode, *Atmospheric Chemistry and Physics*, 12, 10209-10237, [https://doi.org/10.5194/acp-12-10209-](https://doi.org/10.5194/acp-12-10209-2012)
622 2012, 2012.

623 Wesely, M. L.: Parameterization of Surface Resistances to Gaseous Dry Deposition in Regional-Scale
624 Numerical-Models, *Atmospheric Environment*, 23, 1293-1304, [https://doi.org/10.1016/0004-](https://doi.org/10.1016/0004-6981(89)90153-4)
625 6981(89)90153-4, 1989.

626 Xing, J., Mathur, R., Pleim, J., Hogrefe, C., Gan, C. M., Wong, D. C., Wei, C., Gilliam, R., and Pouliot,
627 G.: Observations and modeling of air quality trends over 1990-2010 across the Northern Hemisphere:
628 China, the United States and Europe, *Atmospheric Chemistry and Physics*, 15, 2723-2747, 10.5194/acp-
629 15-2723-2015, 2015.

630 Zhang, L., Brook, J. R., and Vet, R.: A revised parameterization for gaseous dry deposition in air-quality
631 models, *Atmospheric Chemistry and Physics*, 3, 2067-2082, <https://doi.org/10.5194/acp-3-2067-2003>,
632 2003.

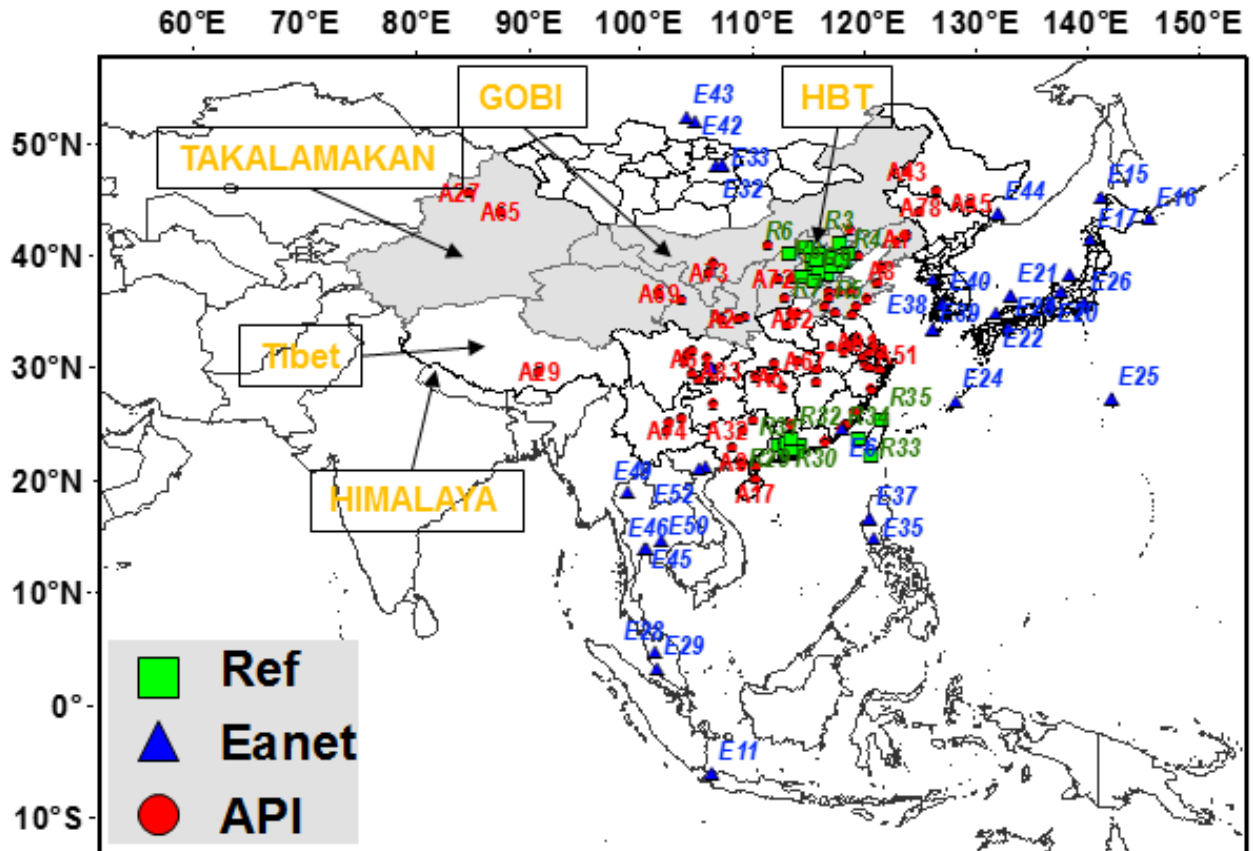
633

634

635 **Figures and tables**

636

637 **Figure 1**



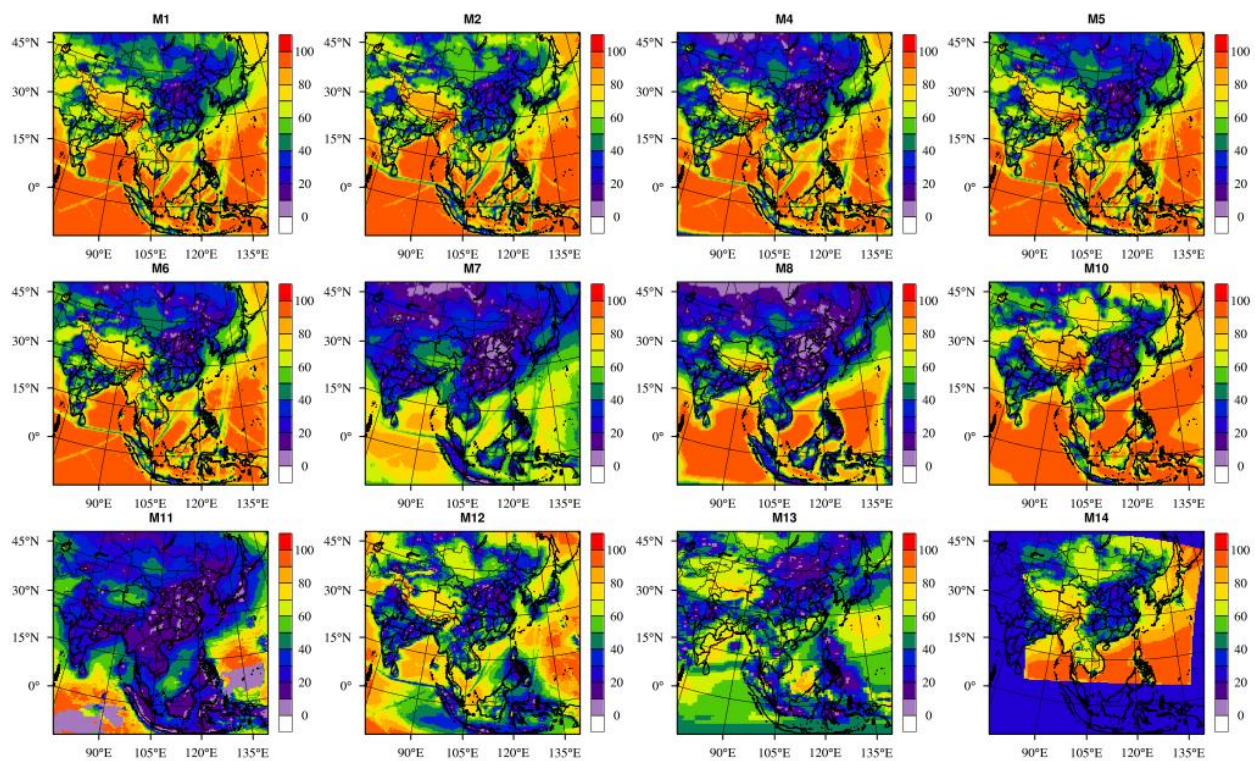
638

639 Figure 1 The geographical locations of observation networks of API (red color, A1-A86), EANET (blue color, E1-

640 E54, only sites with available observation during simulation time are shown) and Ref (green color, R1-R35) sites.

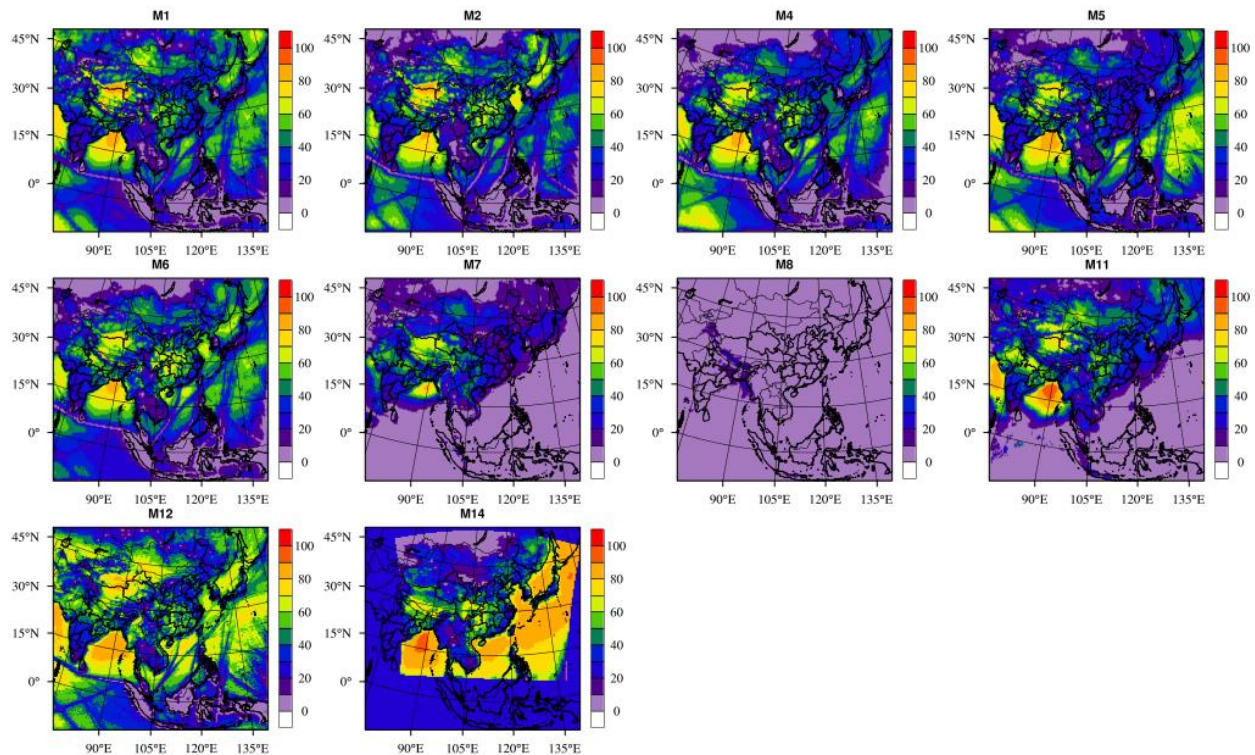
641 Grey shaded regions have been reported to be affected by dust storms.

642 **Figure 2**

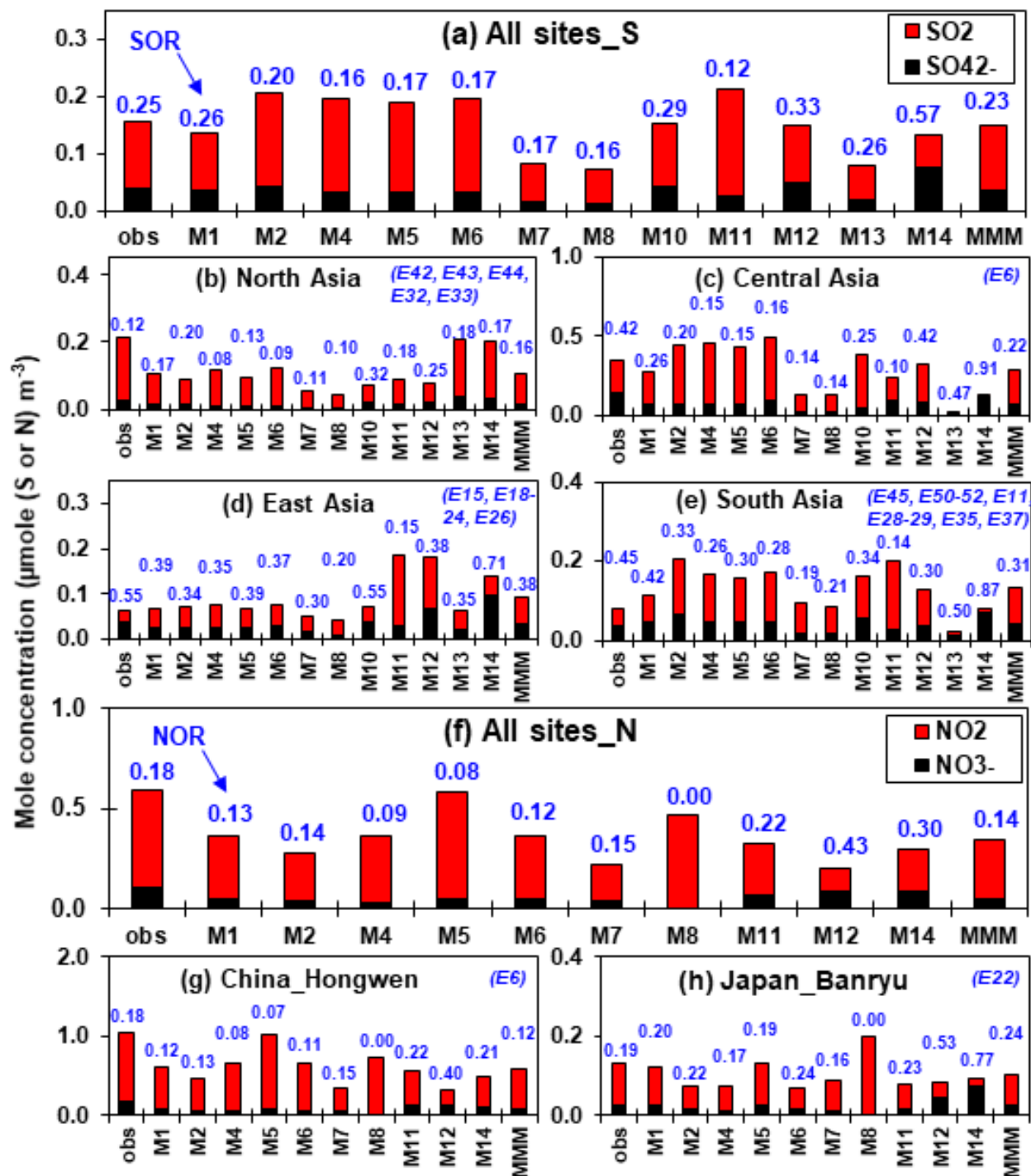


643
644 Figure 2 *SOR* values at surface layer for models (unit: %). *SOR* is calculated by $SO_4^{2-}/(SO_2+SO_4^{2-})\times 100\%$. The SO_2
645 and SO_4^{2-} concentrations are transferred from ppb and $\mu g\ m^{-3}$ to mole(S) m^{-3} before calculating *SOR*. Values are
646 calculated by annual average data.
647

648 **Figure 3**

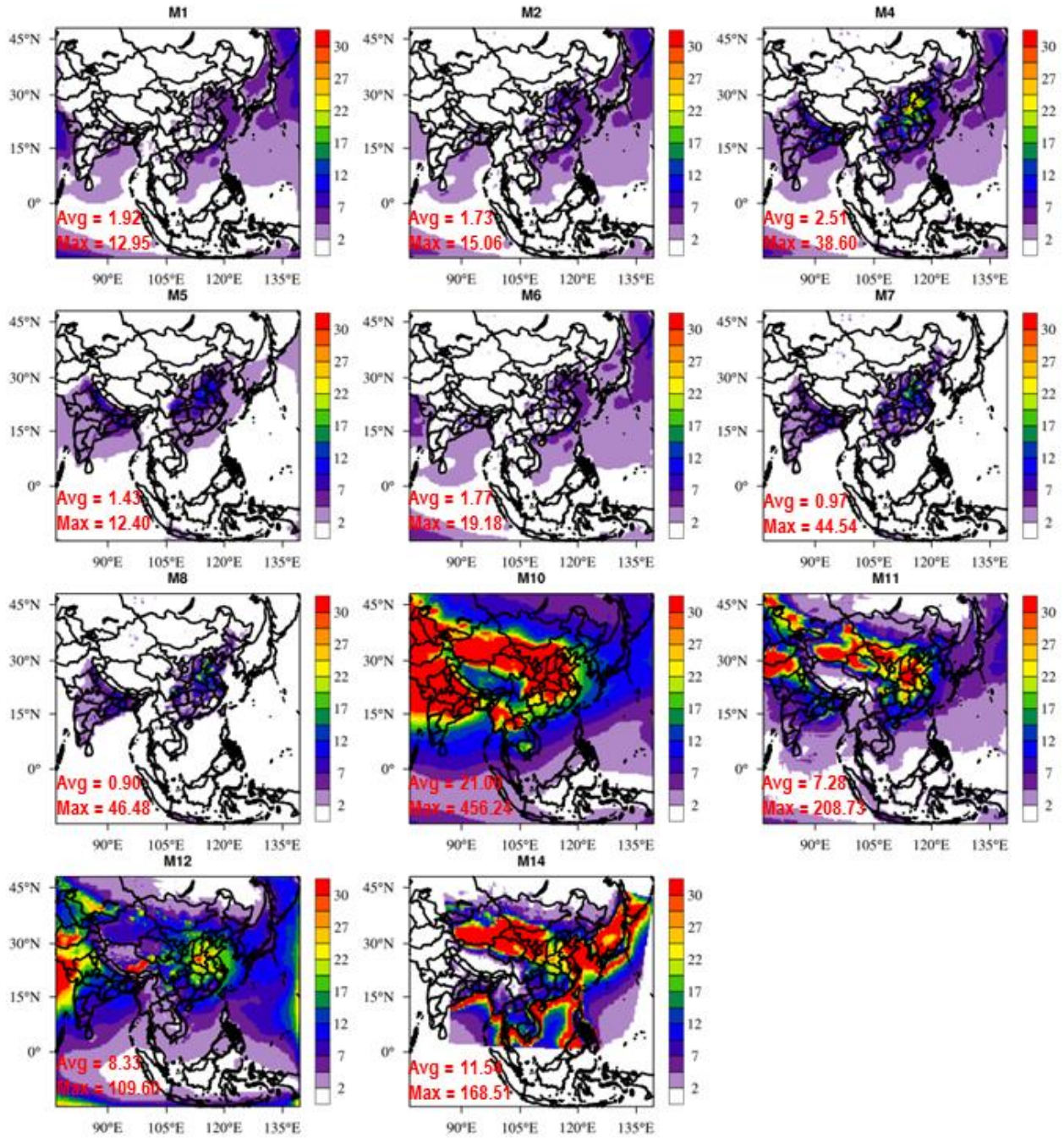


649
650 Figure 3 Same as Fig.2 but for $C(NO_2)$ (unit: %). $C(NO_2)$ is calculated by $NO_3^- / (NO_2 + NO_3^-) \times 100\%$. The $C(NO_2)$ of
651 M8 is extremely low due to unreasonable low NO_3^- concentration, which is considered as outlier in this study. Values
652 are calculated by annual average data.



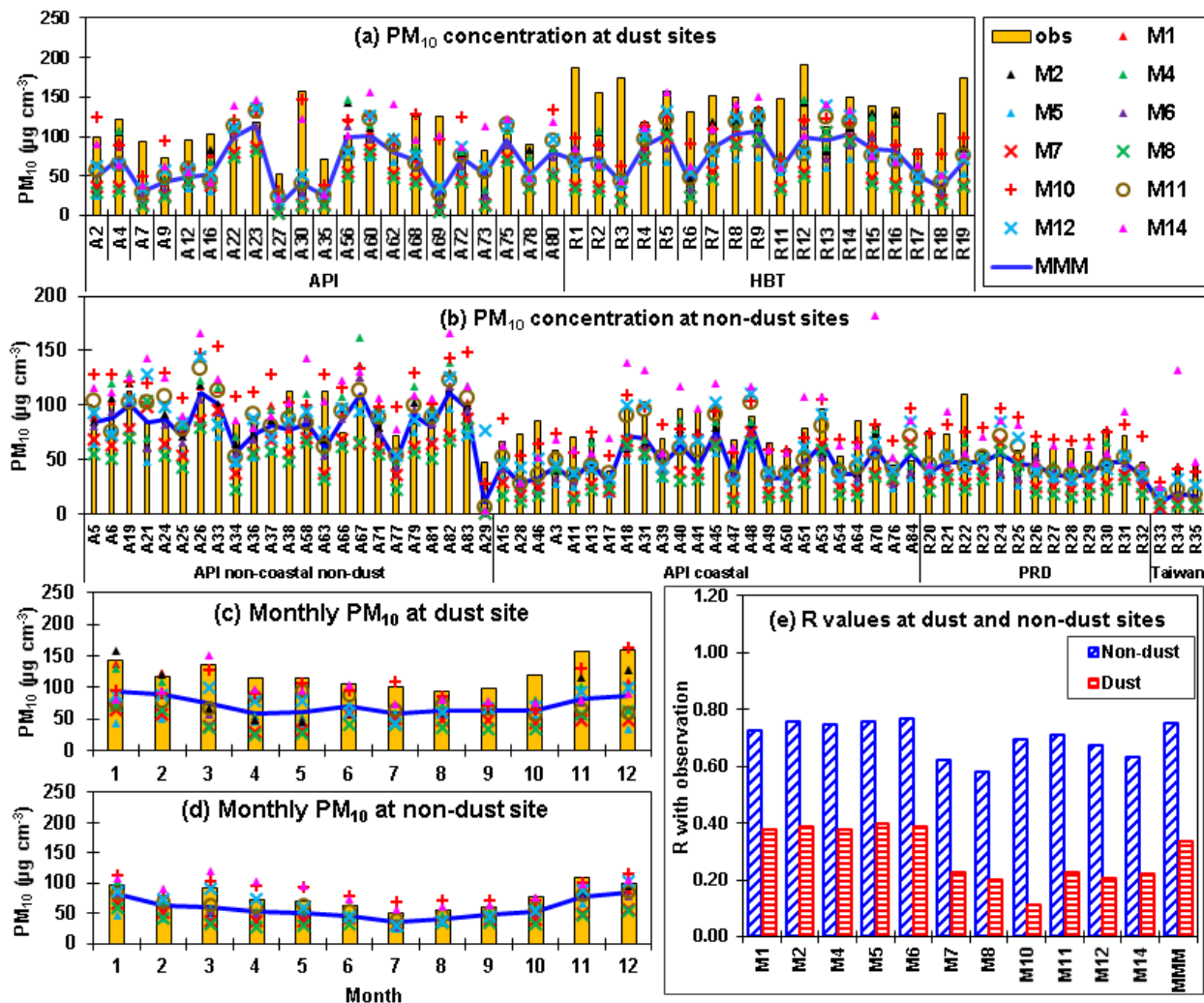
654
 655 Figure 4 Gas-particle conversions of S and N of observation and models at EANET sites. The unit is $\mu\text{mole (S or N)}$
 656 m^{-3} . The red bars and black bars represent the concentrations of gases and aerosols. The blue-color values above the
 657 bars are observed/modelled *SOR* and *C(NO₂)*. Values are calculated with annual average concentrations. The
 658 concentrations of gases and aerosols are all transferred to $\mu\text{mole (S or N)}$ m^{-3} before calculation. The blue-color
 659 numbers on top-right (e.g. E22) are site numbers. The locations of the sites are illustrated in Fig. 1. Results for
 660 individual sites are shown in supplementary Fig. S1.

661 **Figure 5**



662 Figure 5 Annual average PMC concentrations at surface layer of individual models ($\mu\text{g m}^{-3}$). The value is calculated
 663 by subtracting $\text{PM}_{2.5}$ from PM_{10} . The values in left-bottom are domain average (Avg) and maximum (Max) values.
 664
 665

666 **Figure 6**

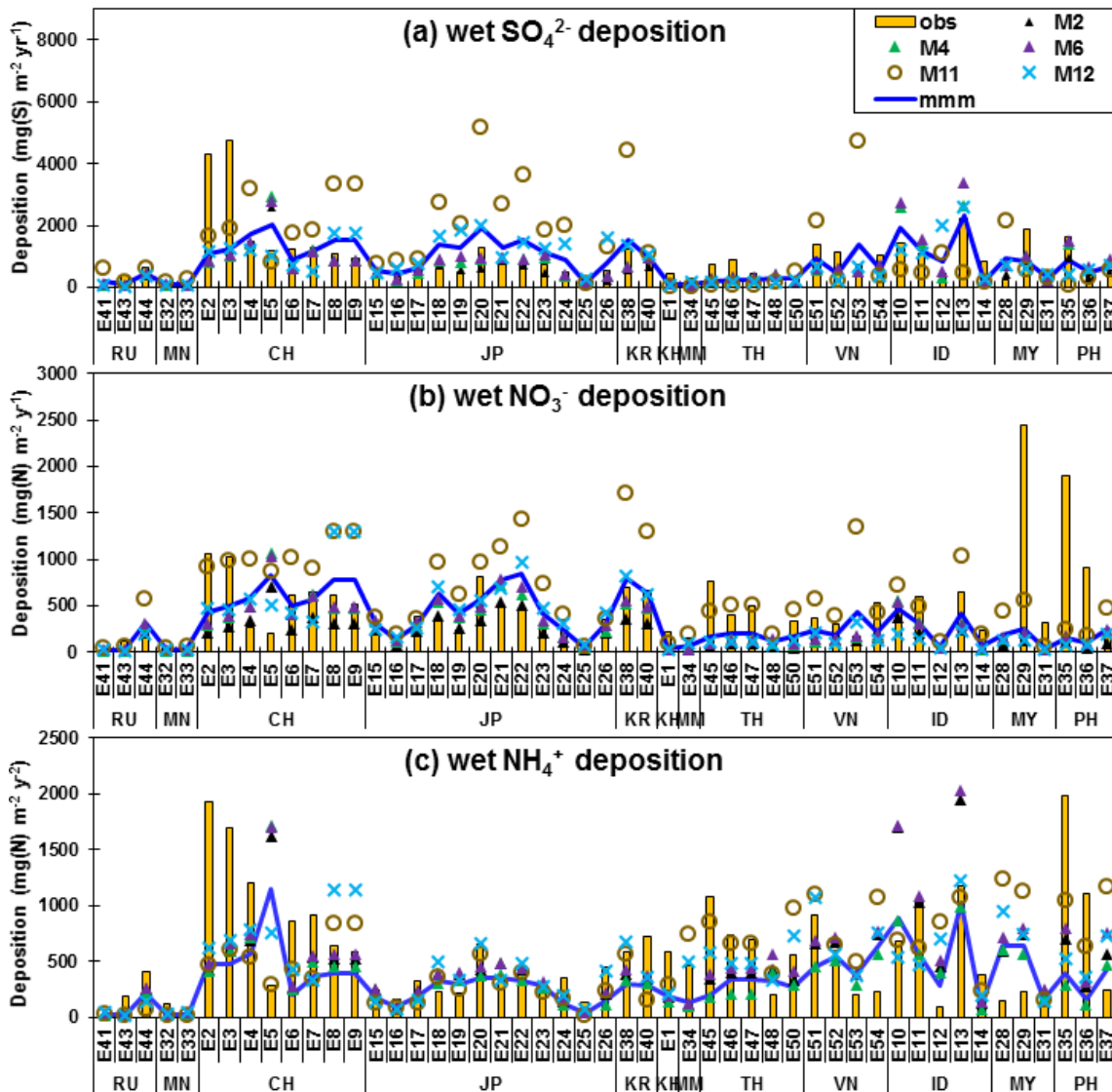


667
 668 Figure 6 Multi-model performances on (a-b) annual average PM₁₀ concentrations at the dust sites and non-dust sites
 669 and (c-d) monthly average PM₁₀ concentrations at the dust sites and non-dust sites. X axis for (a-b) indicates site
 670 numbers. The locations of the sites are illustrated in figure 1. The yellow bars are observations, the blue lines are the
 671 MMM and different markers represent individual model results. (e) R values of models with observations at the dust
 672 and non-dust sites.

673

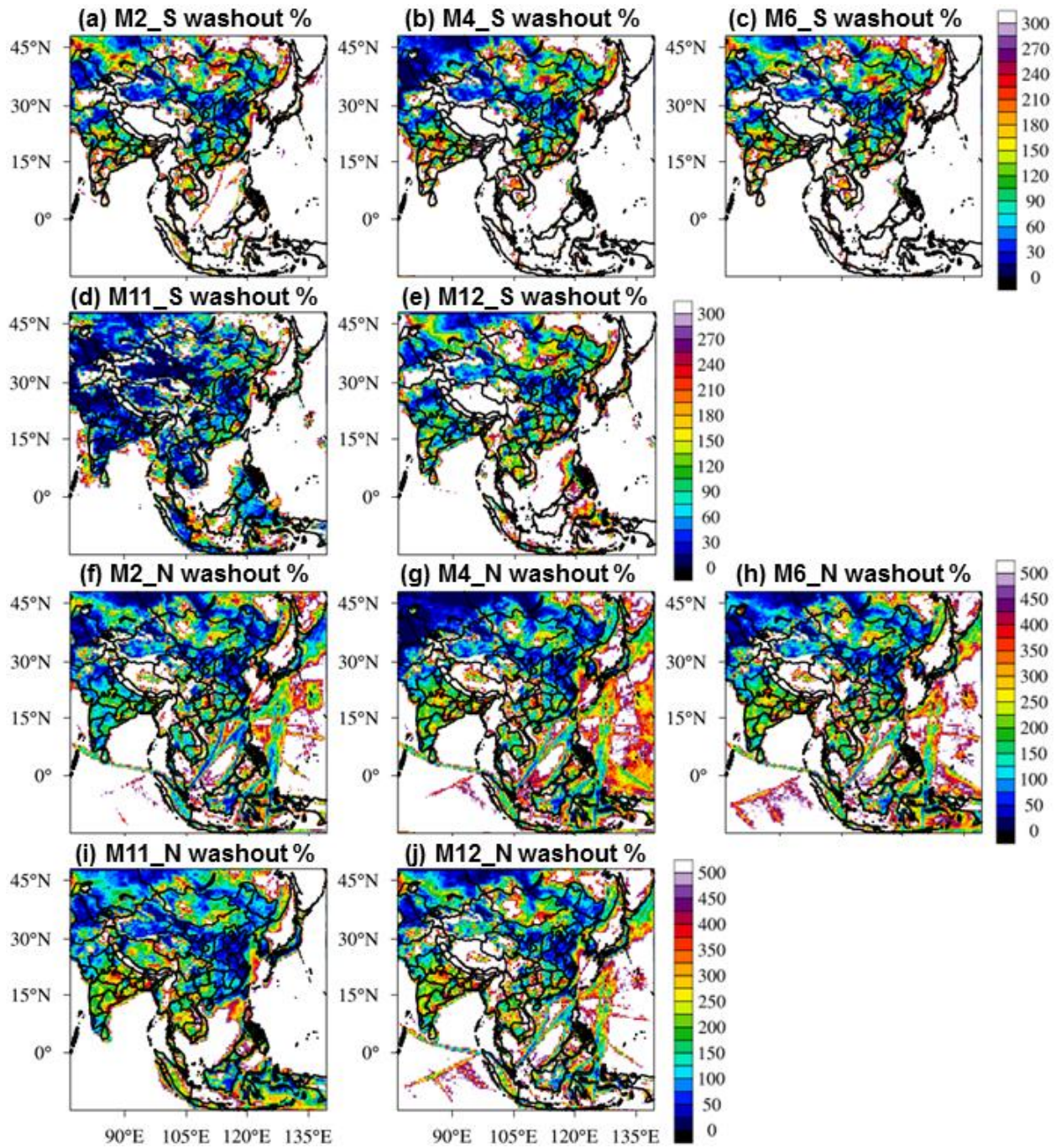
674

675 **Figure 7**



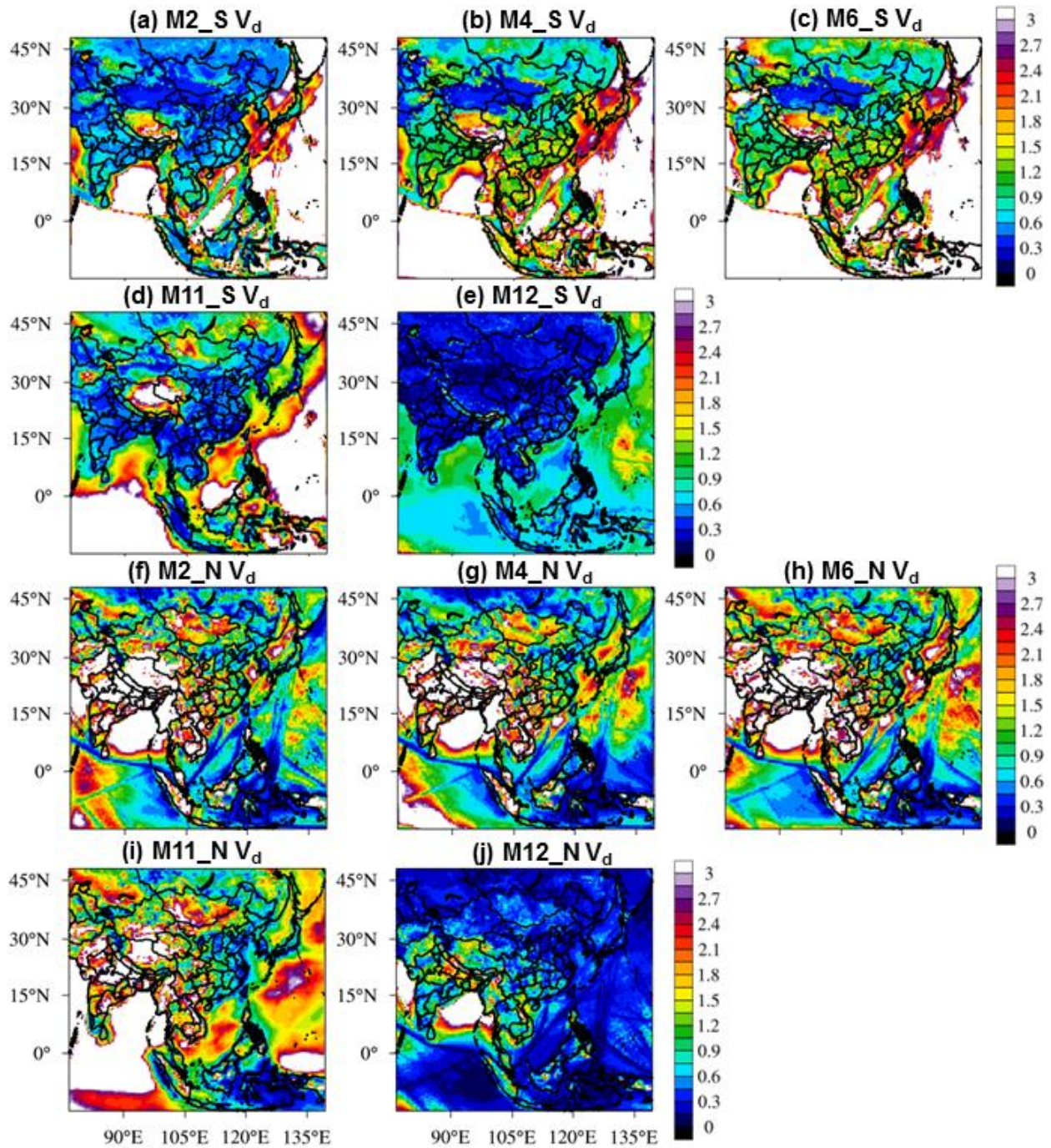
676
 677 Figure 7 Modelled annual-accumulated wet deposition of SO_4^{2-} , NO_3^- and NH_4^+ compared with observation from
 678 EANET network. The units are $\text{mg(S or N) m}^{-2} \text{yr}^{-1}$. Abbreviation for regions: RU-Russia, MN-Mongolia, CH-
 679 China, JP-Japan, KR-Korea, KH-Cambodia, MN-Myanmar, TH-Thailand, VN-Vietnam, ID-Indonesia, MY-
 680 Malaysia, PH-Philippine.
 681

682 **Figure 8**



683
684 Figure 8 Washout ratios (λ_{wet}) of (a-e) S deposition and (f-j) N deposition of models. Values are calculated with
685 annual accumulated depositions. The unit is %.
686

687 **Figure 9**



688 Figure 9 Dry deposition velocities (V_d) of (a-e) S deposition and (f-j) N deposition of models. Values are calculated
689 with annual accumulated depositions. The unit is cm s^{-1} .
690
691

692 **Table 1**693 Table 1 Multi-model performance on annual average concentrations of PM₁₀ at the dust and non-
694 dust sites (unit: $\mu\text{g m}^{-3}$)

Dust site	M1	M2	M4	M5	M6	M7	M8	M10	M11	M12	M14	MMM
Mean Obs	120.7											
Mean MMM	77.2	82.2	81.6	51.7	65.6	47.5	44.3	102.5	73.5	77.3	92.1	69.2
<i>S</i>	0.4	0.4	0.4	0.3	0.3	0.2	0.2	0.1	0.2	0.2	0.3	0.3
<i>MB</i>	-43.5	-38.5	-39.2	-69.0	-55.1	-73.2	-76.4	-18.2	-47.2	-43.4	-28.6	-51.5
<i>R</i>	0.4	0.4	0.4	0.4	0.4	0.2	0.2	0.1	0.2	0.2	0.2	0.3
<i>F</i>	66.7	69.2	69.2	38.5	56.4	35.9	33.3	84.6	59.0	66.7	66.7	66.7
<i>NMB</i> (%)	-36.1	-31.9	-32.4	-57.2	-45.7	-60.6	-63.3	-15.1	-39.1	-36.0	-23.7	-42.6
<i>NME</i> (%)	38.3	35.4	36.4	57.2	46.2	60.6	63.3	32.8	42.3	40.5	36.1	42.7
<i>MFB</i> (%)	-49.4	-44.6	-44.6	-83.4	-64.1	-92.9	-98.8	-19.3	-51.8	-46.8	-31.7	-56.9
<i>MFE</i> (%)	51.8	48.3	48.7	83.4	64.7	92.9	98.8	36.1	55.3	51.7	44.5	56.9
Number of Sites	39											

695

696

Table 1 Continued

Non-dust site	M1	M2	M4	M5	M6	M7	M8	M10	M11	M12	M14	MMM
Mean Obs	77.2											
Mean MMM	58.2	58.5	66.5	45.2	55.2	44.8	39.0	90.0	64.4	66.3	89.5	57.8
<i>S</i>	1.0	1.1	1.2	0.8	1.0	0.7	0.6	1.0	1.0	0.9	1.1	0.9
<i>MB</i>	-19.0	-18.7	-10.8	-32.1	-22.1	-32.5	-38.3	12.7	-12.9	-10.9	12.2	-19.4
<i>R</i>	0.7	0.8	0.7	0.8	0.8	0.6	0.6	0.7	0.7	0.7	0.6	0.8
<i>F</i>	82.5	81.0	84.1	66.7	82.5	52.4	46.0	85.7	90.5	93.7	84.1	82.5
<i>NMB</i> (%)	-24.6	-24.2	-14.0	-41.5	-28.6	-42.0	-49.5	16.5	-16.6	-14.1	15.8	-25.1
<i>NME</i> (%)	30.7	30.7	27.3	41.5	31.4	43.9	50.7	25.7	26.3	26.1	30.8	28.0
<i>MFB</i> (%)	-36.8	-37.5	-25.1	-59.2	-41.8	-62.0	-75.0	13.1	-24.9	-20.3	8.3	-34.6
<i>MFE</i> (%)	42.0	42.8	35.3	59.2	44.4	64.0	76.1	23.4	33.5	31.3	29.1	37.5
Number of Sites	63											

697

698

699 **Table 2**

700 **Table 2 Multi-model performances on wet deposition (unit: mg(S or N) m⁻² y⁻¹)**

	Wet SO ₄ ²⁻ Deposition						Wet NO ₃ ⁻ Deposition					
	M2	M4	M6	M11	M12	MMM	M2	M4	M6	M11	M12	MMM
Mean Obs	931.3	931.3	931.3	931.3	931.3	931.3	460.9	460.9	460.9	460.9	460.9	460.9
Mean MMM	633.7	724.2	775	1313.2	826.2	854.5	187.5	266.7	279.5	597.8	308.3	328
S	0.3	0.3	0.3	0.3	0.2	0.3	0.1	0.1	0.1	0.2	0.1	0.1
MB	-297.7	-207.1	-156.3	381.9	-105.1	-76.9	-273.4	-194.2	-181.4	137	-152.6	-132.9
R	0.5	0.4	0.4	0.2	0.3	0.4	0.1	0.2	0.2	0.2	0.1	0.2
F	61.2	61.2	61.2	24.5	40.8	51	38.8	49	46.9	44.9	38.8	46.9
NMB	-32	-22.2	-16.8	41	-11.3	-8.3	-59.3	-42.1	-39.4	29.7	-33.1	-28.8
NME	49.3	50.2	51.5	117.3	62.8	53.6	66.2	60.9	60.6	78.4	68.8	58.2
MFB	-37.4	-23.4	-15.8	4.6	-11.4	-4.6	-75.8	-49.8	-42.1	25.8	-40.9	-27.6
MFE	57.8	55.9	53.7	93.8	66.7	57.6	84.9	71.2	69.3	61	74.6	62.3
Number of Sites	49	49	49	49	49	49	49	49	49	49	49	49

701

702

Table 2 Continued

	Wet NH ₄ ⁺ Deposition					
	M2	M4	M6	M11	M12	MMM
Mean Obs	558.4	558.4	558.4	558.4	558.4	558.4
Mean MMM	459.9	349.4	497.4	505	478	337.6
S	0.3	0.1	0.3	0.3	0.2	0.2
MB	-98.5	-208.9	-61	-53.4	-80.4	-220.7
R	0.3	0.2	0.3	0.4	0.4	0.3
F	40.8	44.9	44.9	51	46.9	38.8
NMB	-17.6	-37.4	-10.9	-9.6	-14.4	-39.5
NME	64.8	65.5	64.9	58.2	57	63.6
MFB	-21.2	-42.4	-14.4	-18	-12.6	-41.9
MFE	70.7	77.9	69.1	65.9	62.9	76.1
Number of sites	49	49	49	49	49	49

703

704

705 **Table 3**

706 Table 3 Domain-total annual-accumulated S and N depositions of models (Tg(S or N) yr⁻¹).

707 Empty values mean no model submissions or the values are 0.

Model	Wet S deposition				Dry S deposition			
	SO ₂	H ₂ SO ₄	SO ₄ ²⁻	Total Wet S	SO ₂	H ₂ SO ₄	SO ₄ ²⁻	Total Dry S
M1	0.06	-	-	-	-	-	-	-
M2	0.04	-	10.4	10.5	3.4	0.01	0.9	4.3
M4	0.06	-	12.5	12.5	6.6	0.01	1.1	7.6
M5	-	-	-	-	-	-	-	-
M6	0.05	-	13.7	13.8	6.3	0.01	1.4	7.7
M7	-	-	-	-	-	-	-	-
M8	-	-	-	-	-	-	-	-
M10	-	-	-	-	-	-	-	-
M11	1.1	0.3	29.9	31.3	6.9	2.2	1.5	10.6
M12	-	-	16.3	16.3	3.7	-	0.4	4.2
M13	6.0	-	-	-	-	-	-	-
M14	0.02	-	6.2	-	5.4	-	3.2	-

708

709 Table 3 Continued

Model	Wet N deposition					Dry N deposition						
	NO ₃ ⁻	NH ₄ ⁺	HNO ₃	NH ₃	Total Wet N	NO	NO ₂	NO ₃ ⁻	NH ₄ ⁺	HNO ₃	NH ₃	Total Dry N
M1	-	-	-	-	-	-	-	-	-	4.3	6.9	-
M2	4.0	8.3	-	-	12.2	0.03	0.4	0.6	0.6	2.0	7.5	11.0
M4	5.4	7.4	-	-	12.8	0.03	0.3	0.7	0.5	2.8	4.7	9.0
M5	-	-	-	-	-	-	0.5	-	-	-	-	-
M6	5.6	9.1	-	-	14.6	0.02	0.3	0.8	0.7	2.9	6.5	11.1
M7	-	-	-	-	-	-	-	-	-	-	-	-
M8	-	-	-	-	-	-	-	-	-	-	-	-
M10	-	-	-	-	-	-	-	-	-	-	-	-
M11	1.5	2.8	8.1	7.6	20.0	-	-	1.3	2.4	3.3	7.1	14.1
M12	5.4	11.0	-	-	16.5	0.04	0.4	0.4	0.3	0.5	2.2	3.9
M13	-	-	4.1	-	-	-	-	-	-	4.5	4.6	-
M14	-	-	-	-	-	-	-	-	-	-	-	-

710

711